Materials Letters 124 (2014) 4–7

Contents lists available at ScienceDirect

Materials Letters

journal homepage: www.elsevier.com/locate/matlet

Electrochemical investigation of microporous and mesoporous α-Fe_2O_3 particles for lithium-ion batteries

Na Zheng [a], Yuxi Chen [a,*], Xiaobin Deng [a], Zhi-Quan Liu [b], Hongbo Liu [a]

[a] *College of Materials and Engineering, Hunan University, Changsha 410082, PR China*
[b] *Shenyang National Laboratory for Materials Science, Institute of Metal Research, Chinese Academy of Sciences, Shenyang 110016, PR China*

ARTICLE INFO

Article history:
Received 9 October 2013
Accepted 2 March 2014
Available online 11 March 2014

Keywords:
Energy storage and conversion
Lithium ion batteries
Iron oxide
Hydrothermal process
Electron microscopy

ABSTRACT

α-Fe_2O_3 has been regarded as a promising candidate as anode materials for high energy-density lithium-ion batteries, because of its high capacity, low cost and environmental affinity. A facile hydrothermal route has been developed to synthesize monocrystalline microporous and mesoporous α-Fe_2O_3 particles by using anions Cl^- and F^- as pore-formation additives in precursor solution, respectively. Electrochemical investigation indicates that the mesoporous α-Fe_2O_3 particles display higher cyclic stabilities and capacity retentions than the microporous α-Fe_2O_3 particles at different current densities, although their sizes are in micrometer range, which indicate that the mesoporous α-Fe_2O_3 particles are promising anode candidate for high energy-density lithium-ion batteries. Furthermore, this facile hydrothermal route using anion Cl^- or F^- as pore-formation additives may be extended to synthesis of other porous metal oxides.

1. Introduction

α-Fe_2O_3 is of great interest as anode materials for high energy-density lithium-ion batteries (LIBs), because of its attractively high specific capacity (1004 mAh g^{-1}), abundance and environmental affinity [1–5]. The high specific capacity of α-Fe_2O_3 is resulted from a conversion mechanism between α-Fe_2O_3 and Li^+,

$$Fe_2O_3 + 6Li^+ + 6e^- \leftrightarrow 2Fe + 3Li_2O \tag{1}$$

During lithiation process, Li ions intercalate into α-Fe_2O_3 lattice to form a composite of nanosized Fe clusters embedded in Li_2O matrix. Then, the composite delithiates back to α-Fe_2O_3. The lithiation/delithiation of α-Fe_2O_3 induces a volume variation of ca. 87%, and consequently early breakdown of electrodes [6–9], which strongly hindered its applications.

It is generally recognized that synthesizing nanosized α-Fe_2O_3 particles and combining α-Fe_2O_3 particles with carbonaceous materials to form α-Fe_2O_3/C composites are effective ways to improve the electrochemical performance [10]. Furthermore, porous α-Fe_2O_3 is expected to be very effective in accommodating the volume variation of α-Fe_2O_3. Porous α-Fe_2O_3 nanorods have been synthesized and displayed enhanced electrochemical performance [11]. Herein we report a facile hydrothermal synthesis and electrochemical investigations of microporous and mesoporous α-Fe_2O_3 particles obtained using anions Cl^- and F^- as pore-formation additives, respectively. The mesoporous α-Fe_2O_3 exhibits higher cyclic stabilities and capacity retentions than the microporous α-Fe_2O_3 particles.

2. Experimental

0.563 g $FeCl_3$ was dissolved into 70 mL deionized water under continuous stirring. 0.847 g $Fe(NO_3)_3$ and 0.735 g NaF were dissolved into 30 and 40 mL deionized water under continuous stirring, respectively. Then, the NaF solution was added dropwise into the $Fe(NO_3)_3$ solution. The solutions were sealed in 100 mL Teflon-sealed autoclaves, and kept at 170 °C for 4 h. After cooled down to ambient temperature, the products were washed using deionized water and alcohol for at least three times, and then dried in oven at 80 °C overnight. Finally, the products were calcined at 300 °C for 4 h. Hereafter, the products synthesized using $FeCl_3$ and $Fe(NO_3)_3-NaF$ are referred to as C3 and F5, respectively.

The microstructure of the products were characterized by a scanning electron microscope (SEM) (JSM 6700F), transmission electron microscope (TEM) (JEM 2100) and N_2 absorption (ASAP 2020).

Electrodes were prepared by drying a slurry (a mixture of 65 wt% active materials, 25 wt% acetylene black and 10 wt% polyvinylidene fluoride) at 100 °C for 4 h under vacuum. Then, CR2032 coin-type cells were assembled with lithium metal as counter electrodes in an argon-filled glove box. The electrolyte was composed of 1 M $LiPF_6$ dissolved in a mixture of ethylene carbonate (EC), diethyl carbonate (DEC) and methyl ethyl carbonate (MEC) with

---

* Corresponding author. Tel: +86 731 88664018; fax:+86 731 88823554.
E-mail address: ychen@hnu.edu.cn (Y. Chen).

http://dx.doi.org/10.1016/j.matlet.2014.03.001
0167-577X/

volume ratio of 1:1:1. The α-Fe_2O_3 mass in electrodes are in a range of 4 – 5 mg. The discharge – charge measurements were carried out on a battery cycler in a voltage range between 0.01 and 3.00 V (CT 2001A, Land Electronic Co.).

3. Results and discussion

XRD investigation indicates that the products synthesized using $FeCl_3$ and $Fe(NO_3)_3$ – NaF as precursors are the expected hematite α-Fe_2O_3 (inset in Fig. 1(a), JCPDS no. 33-0664). SEM images of C3 and F5 are exhibited in Fig. 1(a) and (b), respectively. The α-Fe_2O_3 particle sizes of C3 are in a range of 100–200 nm. The F5 sample exhibits irregular particle shape, and the dominant particle sizes are in micrometer range in addition to a few particles with sizes less than one micrometer. Inset in Fig. 1(b) is a high-magnification SEM image, which reveals that a lot of slit-shaped mesopores are formed inside the α-Fe_2O_3 particles although a few macropores are visible. Fig. 1(c) and (d) are HREM images of C3 and F5, respectively. Both C3 and F5 exhibit perfect crystal lattices. Insets in Fig. 1(c) and (d) are selected-area electron diffraction patterns taken along the $[\bar{1}11]$ and $[2\bar{8}1]$ zone axes of C3 and F5, respectively, which demonstrate their monocrystalline features.

To investigate pore structure in the α-Fe_2O_3 particles, N_2 absorption measurements were performed at 77 K. The absorption – desorption isotherms of C3 and F5 are exhibited in Fig. 2(a). The BET surface areas of C3 and F5 are 11.3 and 37.5 $m^2\,g^{-1}$, respectively. The absorption branch of C3 is close to type-I isotherm, which indicates presence of micropores. The hysteresis loop of F5 is similar to H4 type, indicating presence of slit-shaped mesopores, which is consistent with SEM observations. The BJH pore size distributions calculated from the absorption isotherms of C3 and F5 are displayed in Fig. 2(b). The pore size distribution of C3 confirms presence of micropores. A mesopore peak with high intensity ranging from ca. 5 to 15 nm is clearly evidenced in F5 curve.

Our previous report revealed that anion Cl^- was effective for micropores formation during hydrothermal synthesis of α-Fe_2O_3 [12], in which anion Cl^- could be absorbed in the positively-charged tunnel-structured ferrihydrites formed by dehydration of $Fe(OH)_3$ [13]. Finally, microporous α-Fe_2O_3 was obtained after hydrothermal synthesis. The anion F^- has higher electronegativity (4.0) than the anion Cl^- (3.0), inducing much stronger pore-formation abilities than the anion Cl^- [14]. Therefore, mesopores were formed in F5.

Electrochemical performances of C3 and F5 were evaluated. Fig. 3(a) and (b) are voltage profiles of C3 and F5 at 0.2 C, respectively. The initial discharge/charge capacities of C3 and F5 are 1240/962 mAh g^{-1} and 1012/833 mAh g^{-1}, respectively. Consequently, the first-cycle coulombic efficiencies of C3 and F5 are 78% and 82%, respectively. The initial irreversible capacity of F5 is only 179 mAh g^{-1}. From the voltage profiles, it also can be seen that the capacity fading of the microporous C3 is faster than the mesoporous F5.

Fig. 3(c) displays charge cyclic performances of C3 and F5 at 0.2 C. The charge capacity of the microporous C3 decreases drastically at first, and then stabilize after 30 cycles. The mesoporous F5 exhibits similar drastic decrease of the charge capacities during the first 30 cycles, and then the charge capacities increase gradually with cycling. At the 100th cycle, the charge capacities of C3 and F5 are 608 and

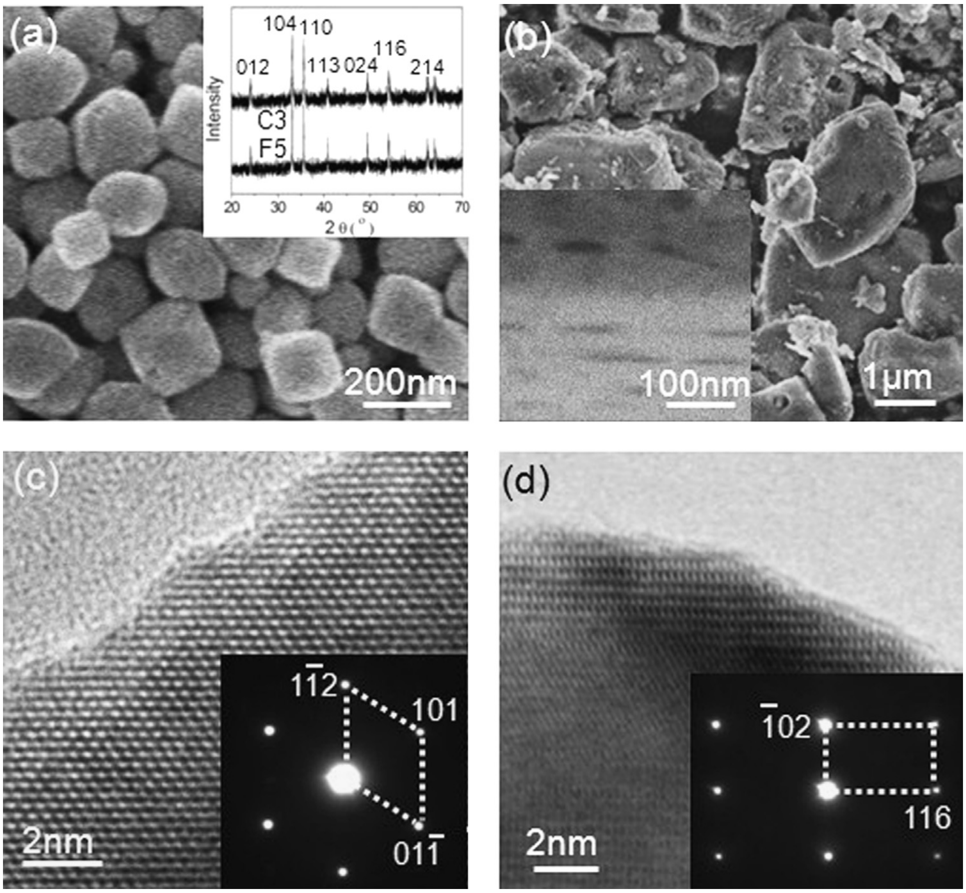

Fig. 1. SEM images of (a) C3 and (b) F5. Inset in (a) is XRD patterns of C3 and F5. Inset in (b) is a high-magnification SEM image. HREM images of (c) C3 and (d) F5. Insets in (c) and (d) are selected-area electron diffraction patterns of C3 and F5, respectively.